Real-time predictions of geomagnetic storms and substorms: Use of the Solar Wind Magnetosphere-Ionosphere System model

M. L. Mays,[1] W. Horton,[1] E. Spencer,[2] and J. Kozyra[3]

Received 5 December 2008; revised 28 April 2009; accepted 7 May 2009; published 2 July 2009.

[1] A low-dimensional, plasma physics-based, nonlinear dynamical model of the coupled magnetosphere-ionosphere system, called Real-Time Solar Wind Magnetosphere-Ionosphere System (WINDMI), is used to predict *AL* and *Dst* values approximately 1 h before geomagnetic substorm and storm event. Subsequently, every 10 min ground-based measurements compiled by World Data Center, Kyoto, are compared with model predictions (http://orion.ph.utexas.edu/~windmi/realtime/). WINDMI model runs are also available at the Community Coordinated Modeling Center (http://ccmc.gsfc.nasa.gov/). The performance of the Real-Time WINDMI model is quantitatively evaluated for 22 storm/substorm event predictions from February 2006 to August 2008. Three possible input solar wind-magnetosphere coupling functions are considered: the standard rectified coupling function, a function due to Siscoe, and a recent function due to Newell. Model *AL* and *Dst* predictions are validated using the average relative variance (ARV), correlation coefficient (COR), and root mean squared error (RMSE). The Newell input function yielded the best model *AL* predictions by all three measures (mean ARV, COR, and RMSE), followed by the rectified, then Siscoe input functions. Model *AL* predictions correlate at least 1 standard deviation better with the *AL* index data than a direct correlation between the input coupling functions and the *AL* index. The mean *Dst* ARV results show better prediction performance for the rectified input than the Siscoe and Newell inputs. The mean *Dst* COR and RMSE measures do not readily distinguish between the three input coupling functions.

Citation: Mays, M. L., W. Horton, E. Spencer, and J. Kozyra (2009), Real-time predictions of geomagnetic storms and substorms: Use of the Solar Wind Magnetosphere-Ionosphere System model, *Space Weather*, *7*, S07001, doi:10.1029/2008SW000459.

1. Introduction

[2] The rapid forecasting of magnetospheric storms and substorms from solar wind data with reliable models is of wide interest and important for protecting the space infrastructure of communication and global positioning spacecrafts. There are basic constraints from plasma physics that forecasting models must observe. The models need to forecast the standard geomagnetic indices used to define substorms and storms such as the *AL* and *Dst* indices. The *AL* index is commonly used as an indication of the intensity of substorms, while the *Dst* index characterizes storm activity and is a measure of the energy stored in the Earth's ring current.

[3] The *AL* index is derived from measurements of the horizontal component of the Earth's magnetic field at stations located along the auroral oval in the Northern hemisphere [*Rostoker*, 1972]. The *AL* index is compiled every minute over a 24 h period in a day and is obtained by selecting the most negative values measured among 12 stations located along the auroral zone, all of them above 50° latitude. The most negative values are taken to be the strongest activity of the westward auroral electrojet which is given by the region 1 field aligned current in the model, that closes in the nightside magnetosphere through the nightside auroral ionosphere. The *Dst* index is obtained from the measurement of the Earth's magnetic field from observatories that are sufficiently distant from the auroral and equatorial electrojets and located at approximately ±20° latitude, while being evenly distributed in longitude

[1]Institute for Fusion Studies, University of Texas at Austin, Austin, Texas, USA.
[2]Center for Space Engineering, Utah State University, Logan, Utah, USA.
[3]Department of Atmospheric, Oceanic, and Space Sciences, University of Michigan at Ann Arbor, Ann Arbor, Michigan, USA.

[*Sugiura*, 1964]. In this paper, the *Dst* index is compared to the output from the Solar Wind Magnetosphere-Ionosphere System (WINDMI) model through the ring current energy W_{rc} using the Dessler-Parker-Schopke relation [*Dessler and Parker*, 1959].

[4] There are many models for the *Dst*, including *Burton et al.* [1975], *Klimas et al.* [1998], *O'Brien and McPherron* [2000], and *Temerin and Li* [2002, 2006]. Models for the electrojet currents and the *AL* index include *Bargatze et al.* [1985], *Klimas et al.* [1992, 1994], and *Li et al.* [2007]. *Temerin and Li* [2006] have reported a high accuracy in *Dst* prediction with COR = 0.956, PE = 0.914, and RMSE = 6.65 nT for the period of 1995–2002. The complex empirical *AL* model of *Li et al.* [2007] achieves COR = 0.795, PE = 0.524, and RMSE = 88 nT for 1997–2001. The comparison of Real-Time WINDMI with other *AL* and *Dst* models is being considered for analysis as model results during solar maximum are accumulated.

[5] In this work, analysis of first results from Real-Time WINDMI model for 22 storm and substorm events from February 2006 to May 2008 is presented. In section 2 the WINDMI model and how it has been extended to run in real time is discussed. Event selection is discussed and Real-Time WINDMI model *AL* and *Dst* prediction performance is evaluated using statistical measures for three candidate input solar wind-magnetosphere coupling functions in section 3. The 14–18 December 2006 storm and substorm event is discussed in more detail in section 4. In section 5 discussions and future model uses and enhancements are presented.

2. WINDMI Model Description

[6] WINDMI is a low-dimensional ($d = 8$) plasma physics-based model of the coupled magnetosphere ionosphere system [*Horton and Doxas*, 1996]. The nonlinear system of ordinary differential equations describes the energy transfer between the basic components of the system: the geotail lobe with associated current I and voltage V, the central plasma sheet with pressure p and parallel kinetic energy $K_{||}$, the ring current with energy W_{rc}, the nightside region 1 current I_1 with voltage V_I, and the nightside region 2 current I_2 that closes as the partial ring current [*Horton and Doxas*, 1998; *Spencer et al.*, 2007]. Of the eight dynamical variables determined by the model, the region 1 field aligned current I_1 and the ring current plasma energy W_{rc} can be compared the *AL* and *Dst* indices. The input to the model is the solar wind driving voltage V_{sw} coupling function. The equations for the state vector $X = (I, V, p, K_{||}, I_1, V_I, I_2, W_{rc})$ in the WINDMI model are given by

$$L\frac{dI}{dt} = V_{sw}(t) - V + M\frac{dI_1}{dt}, \tag{1}$$

$$C\frac{dV}{dt} = I - I_1 - I_{ps} - \Sigma V, \tag{2}$$

$$\frac{3}{2}\frac{dp}{dt} = \frac{\Sigma V^2}{\Omega_{cps}} - u_0 p K_{||}^{1/2}\Theta(u) - \frac{pVA_{eff}}{\Omega_{cps}B_{tr}L_y} - \frac{3p}{2\tau_E}, \tag{3}$$

$$\frac{dK_{||}}{dt} = I_{ps}V - \frac{K_{||}}{\tau_{||}}, \tag{4}$$

$$L_I\frac{dI_1}{dt} = V - V_I + M\frac{dI}{dt}, \tag{5}$$

$$C_I\frac{dV_I}{dt} = I_1 - I_2 - \Sigma_I V_I, \tag{6}$$

$$L_2\frac{dI_2}{dt} = V_I - (R_{prc} + R_{A2})I_2, \tag{7}$$

$$\frac{dW_{rc}}{dt} = R_{prc}I_2^2 + \frac{pVA_{eff}}{B_{tr}L_y} - \frac{W_{rc}}{\tau_{rc}}. \tag{8}$$

The 18 physical parameters of WINDMI are approximated semianalytically or from data and the nominal values are shown in Table 1. The parameters can also be optimized (against the Quicklook *Dst* data) within physically allowable ranges, using a genetic algorithm. The optimized results are only meaningful when the real-time Quicklook *Dst* data is available and reliable. The nominal parameters, genetic algorithm procedure, and calculation of the model prediction for the *AL* and *Dst* indices are described in detail by *Spencer et al.* [2007]. For this work the nominal values of the parameters are used for all events.

[7] Real-time measurements of solar wind proton density n_{sw}, solar wind velocity v_{bulk}, and interplanetary magnetic field (IMF) B_{IMF} are available from the ACE spacecraft [*Stone et al.*, 1998] in 1 min intervals. The ACE spacecraft has a halo orbit about the L1 Lagrange point located approximately 1.5×10^6 km from the Earth. The data is time delayed using the formula $t_{delay} = (X_{ACE} - \overline{X}_{MP})/\overline{v}_{bulk}$ where X_{ACE} is the average x coordinate of the ACE spacecraft in GSM coordinates, X_{MP} is the average magnetopause standoff distance over the storm period calculated from the *Shue et al.* [1997] formula, and $\overline{v}_{bulk}$ is the average solar wind bulk velocity for the duration of the event. The more accurate time delay formulas of *Weimer et al.* [2003]; *Bargatze et al.* [2005] are being implemented for future studies.

[8] These quantities are used to derive a series of input solar wind driving voltages for the WINDMI model. There are several candidate coupling functions for the driving voltage and three are considered in this work: the rectified, Siscoe, and Newell coupling functions.

[9] The rectified driving voltage [*Burton et al.*, 1975; *Reiff and Luhmann*, 1986] is given by $v_{bulk}B_S^{IMF}L_y^{eff}$, where v_{bulk}

Table 1. WINDMI Nominal Parameters[a]

Parameter	Value	Description
L	90 H	Inductance of the lobe cavity surrounded by the geotail current $I(t)$.
M	1 H	The mutual inductance between the nightside region 1 current loop I_1 and the geotail current loop I.
C	50000 F	Capacitance of the central plasma sheet in Farads.
Σ	8 S	Large gyroradius ρ_i plasma sheet conductance from the quasineutral layer of height $(L_z\rho_i)^{1/2}$ about the equatorial sheet.
Ω_{cps}	2.6×10^{24} m^3	Volume of the central plasma sheet that supports mean pressure $p(t)$, initial estimate is $10^4 R_E^3$.
u_0	4×10^{-9} m^{-1}kg$^{-1/2}$	Heat flux limit parameter for parallel thermal flux on open magnetic field lines $q_\parallel$ = const $\times$ $v_\parallel p = u_0(K_\parallel)^{1/2}p$. The mean parallel flow velocity is $(K_\parallel/(\rho_m\,\Omega_{cps}))^{1/2}$.
I_c	1.78×10^7 A	The critical current above which unloading occurs.
α	8×10^{11}	The geotail current driven by the plasma pressure p confined in the central plasma sheet. Pressure balance between the lobe and the central plasma sheet gives $B_\ell^2/2\mu_0 = p$ with $2L_x\,B_\ell = \mu_0 I_{ps}$. This defines the coefficient α in $I_{ps} = \alpha p^{1/2}$ to be approximately $\alpha = 2.8\,L_x/\mu_0^{1/2}$.
$\tau_\parallel$	10 min	Confinement time for the parallel flow kinetic energy $K_\parallel$ in the central plasma sheet.
τ_E	30 min	Characteristic time of thermal energy loss through earthward and tailward boundary of plasma sheet.
L_1	20 H	The self inductance of the wedge current or the nightside region 1 current loop $I_1(t)$
C_I	800 F	The capacitance of the nightside region 1 plasma current loop.
Σ_I	3 mho	The ionospheric Pedersen conductance of the westward electrojet current closing the I_1 current loop in the auroral (altitude ~100 km, 68°) zone ionosphere.
R_{prc}	0.1 ohm	The resistance of the partial ring current.
τ_{rc}	12 h	The decay time for the ring current energy.
L_2	8 H	The inductance of the region 2 current.
R_{A2}	0.3 ohm	Resistance of the region 2 footprint in the auroral region.
B_{tr}	5×10^{-9} T	The magnetic field in the transition region.
A_{eff}	8.14×10^{13} m^2	The average effective area presented to the geotail plasma for plasma entry into the inner magnetosphere, estimated to be $2R_E^2$.
L_y	3.2×10^7 m	The effective width of the Alfven layer aperture, estimated to be $5R_E$.
ΔI	1.25×10^5 A	The rate of turn on of the unloading function.

[a]Estimated by physical considerations of the state and geometry of the nightside magnetosphere using the Tsyganenko magnetic field model.

is solar wind bulk velocity in GSM coordinates, B_S^{IMF} is the southward IMF component and $L_y^{eff} \approx 10\ R_E$ is an effective cross-tail width over which the dynamo voltage is produced. The half-wave rectifier has a base voltage of 40 kV for northward IMF $B_z^{IMF} \geq 0$ and for southward IMF $B_z^{IMF} < 0$ the driving voltage is

$$V_{sw}^{Bs} = 40(\mathrm{kV}) + v_{bulk} B_s^{IMF} L_y^{eff}. \quad (9)$$

[10] The second coupling function is given by *Siscoe et al.* [2002a, 2002b] and *Ober et al.* [2003] as the potential drop around the magnetopause from magnetic reconnection in the absence of saturation mechanisms. The formula is given by

$$V_{sw}^{S}(\mathrm{kV}) = 30.0(\mathrm{kV}) + 57.6 E_{sw}(\mathrm{mV/m}) P_{sw}^{-1/6}(\mathrm{nPa}), \quad (10)$$

where $E_{sw} = v_{bulk} B_T \sin(\frac{\theta}{2})$ is the solar wind electric field with respect to the magnetosphere and the dynamic solar wind pressure $P_{sw} = n_{sw}\ m_p v_{bulk}^2$. The perpendicular component of the the magnetic field is given by $B_T = (B_y^2 + B_z^2)^{1/2}$. Here m_p is the mass of a proton and only the proton density contribution has been included in n_{sw}. The IMF clock angle θ is given by $\tan^{-1}(B_y/B_z)$.

[11] The third coupling function by *Newell et al.* [2007, 2008] represents rate of magnetic flux $d\,\Phi_{MP}/dt$ opening at the magnetopause

$$d\Phi_{MP}/dt = v_{bulk}{}^{4/3} B_T^{2/3} \sin\left(\frac{\theta}{2}\right)^{8/3}, \quad (11)$$

which gives the driving voltage

$$V_{sw}^{N} = 40(\mathrm{kV}) + \nu d\Phi_{MP}/dt. \quad (12)$$

The scaling factor $\nu = \overline{V_{sw}^{Bs}}/\overline{d\Phi_{MP}/dt}$ is the ratio of the average rectified voltage to the magnetic flux for the storm period.

[12] Every 10 min the data and and WINDMI model predictions for the concurrent runs are shown on the website: http://orion.ph.utexas.edu/~windmi/realtime/. WINDMI model runs can also be requested from the Community Coordinated Modeling Center (http://ccmc.gsfc.nasa.gov/). For this work the trigger threshold for storm activity is set to a *Dst* level of below −50 nT and for substorm activity the trigger threshold is set to an *AL*

Table 2. List of 22 Events for Which Storms and/or Substorms Have Been Predicted by Real-Time WINDMI From February 2006 to August 2008[a]

	Data		Real-Time WINDMI[b]	
Date	Minimum *Dst* (nT)	Minimum *AL* (nT)	*Dst* (nT)	Minimum *AL* (nT)
2–8 Apr. 2006[c]	−87	−1179	−26/−40/−45	−270/−341/−267
8–11 Apr. 2006	−80	−1045	−40/−35/−47	−402/−395/−461
13–18 Apr. 2006	−111	−1598	−125/−134/−122	−1123/−1000/−1017
6–9 Aug. 2006	−44	−1556	−31/−42/−46	−398/−406/−465
17–23 Aug. 2006	−71	−1697	−68/−56/−87	−758/−426/−811
23–26 Sep. 2006[c]	−56	−1167	−20/−27/−30	−347/−307/−380
20–22 Oct. 2006[c]	−28	−822	−17/−33/−27	−224/−348/−320
9–12 Nov. 2006	−51	−622	−37/−43/−45	−709/−436/−460
29 Nov. to 1 Dec. 2006	−74	−1704	−49/−47/−63	−432/−370/−451
5–8 Dec. 2006[c]	−48	−1175	−28/−34/−40	−386/−318/−379
14–18 Dec. 2006	−146	−2349	−180/−193/−228	−1779/−1423/−1752
28–31 Jan. 2007	−40	−1296	−30/−38/−38	−533/−428/−506
22–27 Mar. 2007	−69	−1032	−43/−36/−66	−400/−348/−602
31 Mar. to 4 Apr. 2007	−63	−813	−27/−26/−37	−380/−332/−401
16–19 Apr. 2007[c]	−47	−584	−22/−38/−37	−311/−381/−385
27 Apr. to 1 May 2007	−56	−942	−29/−32/−43	−399/−349/−454
21–26 May 2007	−63	−1259	−54/−48/−61	−736/−437/−699
10–13 Jul. 2007	−40	−896	−27/−35/−58	−375/−350/−814
13–17 Jul. 2007	−46	−891	−38/−33/−63	−410/−342/−746
25–28 Oct. 2007	−51	−1047	−25/−32/−37	−364/−381/−436
19–23 Nov. 2007	−71	−1552	−41/−82/−57	−654/−855/−716
7–10 Mar. 2008	−72	−1332	−39/−37/−50	−937/−440/−856

[a]The WDC, Kyoto, minimum *Dst* and *AL* data for each event are given. The *AL* data are provisional, the *Dst* data are provisional up to January 2007, and from January 2007 onward the *Dst* data are Quicklook. The minimum Real-Time WINDMI *Dst* and *AL* predictions are given for the rectified, Siscoe, and Newell input drivers are given.

[b]Here the first value is the result using rectified input driver V_{sw}^{Bs} (equation (9)), the second value is the result using the Siscoe input driver V_{sw}^{S} (equation (10)), and the third value is the result using the Newell input driver V_{sw}^{N} (equation (12)).

[c]The model *AL* and *Dst* did not reach the defined activity threshold for the alerts and were not detected. They are close to the thresholds and are included here for statistical analysis.

level of below −500 nT. There is an automated email alert system which notifies of predicted activity.

3. Real-Time WINDMI Results: February 2006 to August 2008

3.1. Event Selection

[13] Twenty-two storms and or substorm events between February 2006 to August 2008 were selected for model performance analysis. The events are shown in Table 2 and were selected on the basis of Real-Time WINDMI results triggering on a threshold of $Dst \leq -50$ nT or $AL \leq -400$ nT. This is only a subset of larger substorm events between February 2006 to August 2008 that meet this criteria and there were many other mostly smaller substorm events during this period that are not well defined. The time interval was selected such that the initial, main, and recovery phases of the *Dst* signature were included. The time interval must also include any *AL* activity above 400 nT but starts and ends with a ''quiet time'' *AL* of less than 100–200 nT.

[14] The World Data Center (WDC), Kyoto, minimum *Dst* and *AL* data and Real-Time WINDMI minimum *Dst* and *AL* predictions for both input drivers are also shown in Table 2. Seven of the 22 events had sudden storm commencement. The mean *Dst* index data is −64.3 nT and and the mean *AL* index is −1252.6 nT for these selected events. The time interval chosen for each event was determined using both *AL* and *Dst* data. The time interval used to evaluate model performance was a subset of each event only during a shorter period around which storm or substorm activity was above the threshold. For each event, the given activity time range was fixed for both *AL* and *Dst* comparisons.

3.2. Model Performance

[15] Concurrent runs of the Real-Time WINDMI model are performed using the input solar wind rectified driver, Siscoe driver, or Newell driver with WINDMI model nominal parameters. The model parameters are held fixed for all driver inputs and events and therefore variations in the model output are due to differences in the driving voltage. The performance of the model was measured with the average relative variance (ARV), correlation coefficient (COR), and root mean squared error (RMSE) for each event. These metrics are defined in Appendix A. In this work ACE Level 2 data was used in the calculations instead of ACE real-time data which is normally used on the Real-Time WINDMI website. WDC, Kyoto, *AL* and *Dst* data and model comparisons were calculated using provisional values when available. For this work, provisional *AL* data was available for all of the events, *Dst* data was provisional up to January 2007, and so Quicklook *Dst* data was used for the remaining events.

Table 3. Mean ARV Measures of Real-Time WINDMI Model Results[a]

Input	Mean *AL* ARV	Mean *Dst* ARV
Rectified V_{sw}^{Bs}	0.38 ± 0.21	0.37 ± 0.27
Siscoe V_{sw}^{S}	0.41 ± 0.16	0.42 ± 0.23
Newell V_{sw}^{N}	0.33 ± 0.17	0.54 ± 0.39

[a]For the selected events from February 2006 to August 2008 (listed in Table 2). The ARV is calculated using equation (A1) in Appendix A.

[16] The mean *AL* and *Dst* ARV of all of the events is shown in Table 3 for the three input coupling functions. In Table 4 the mean *AL* and *Dst* correlation coefficient is shown. For the 22 events, the *AL* prediction performance has a mean ARV = 0.38 ± 0.21 and COR = 0.62 ± 0.13 using the rectified voltage as input. When the Siscoe voltage is used as input the mean *AL* ARV = 0.41 ± 0.16 and COR = 0.52 ± 0.15. The Newell input coupling function has the best *AL* performance of the three with a mean ARV = 0.33 ± 0.17 and COR = 0.64 ± 0.12.

[17] The best *Dst* prediction is obtained from the rectified input voltage with a mean ARV = 0.37 ± 0.27 and COR = 0.80 ± 0.12. For Siscoe voltage input the mean *Dst* ARV = 0.42 ± 0.23 and COR = 0.77 ± 0.13. The mean *Dst* ARV = 0.54 ± 0.39 and COR = 0.79 ± 0.14 results for the Newell input show that the Newell input coupling function did not perform as well as the rectified and Siscoe input. However, the mean *Dst* COR for all three input functions are very similar with only a few percent differences.

[18] Table 4 also shows the direct correlation coefficient of the *AL* index with the input solar wind driving voltage (calculated from data) in the third column. The direct correlation of *Dst* index with the input driving voltage is not shown as the model *Dst* will always have a higher correlation with the *Dst* index data than the input coupling function, because the *Dst* a time integrated index. The mean direct correlation coefficient for the *AL* is COR = 0.40 ± 0.20 with the rectified, COR = 0.37 ± 0.18 for the Siscoe input, and COR = 0.42 ± 0.18 for the Newell input. The model *AL* correlates with the *AL* index data at least one standard deviation better than a direct correlation of each coupling function with the *AL* data.

[19] The mean RMSE of the events is shown in Table 5 and the values confirm the ARV and COR comparisons of the three coupling functions. The *AL* prediction has an average RMSE = 111.5 ± 39.5 nT, 126.1 ± 52.4 nT, and 125.2 ± 45.5 nT for the Newell, rectified, and Siscoe input voltages, respectively. For the *Dst* prediction the average RMSE = 9.8 ± 3.4, 10.7 ± 4.0, and 11.9 ± 6.9 nT for the rectified, Siscoe, and Newell coupling functions.

Table 4. Mean COR of Real-Time WINDMI Model Results[a]

Input	Mean *AL* COR	Mean *AL* Direct COR	Mean *Dst* COR
Rectified V_{sw}^{Bs}	0.62 ± 0.13	0.40 ± 0.20	0.80 ± 0.12
Siscoe V_{sw}^{S}	0.52 ± 0.15	0.37 ± 0.18	0.77 ± 0.13
Newell V_{sw}^{N}	0.64 ± 0.12	0.42 ± 0.18	0.79 ± 0.14

[a]For the selected events from February 2006 to August 2008 (listed in Table 2). The mean direct correlation between the calculated input driving voltage V_{sw} and the *AL* index is shown. The COR is calculated using equation (A2) in Appendix A.

Table 5. Mean Values of the RMSE of Real-Time WINDMI Model Results[a]

Input	Mean *AL* RMSE	Mean *Dst* RMSE
Rectified V_{sw}^{Bs}	123.2 ± 52.4	9.8 ± 3.4
Siscoe V_{sw}^{S}	126.1 ± 45.5	10.7 ± 4.0
Newell V_{sw}^{N}	111.5 ± 39.5	11.9 ± 6.9

[a]For the selected events from February 2006 to August 2008 (listed in Table 2). The RMSE is calculated using equation (A3) in Appendix A.

[20] Storm prediction can also be assessed from the statistical decision process perspective. Using the storm event selection criteria we define "correct" to mean the data $Dst \leq -50$ nT and the model was also $Dst \leq -50$ nT. The type I error or "false negative" means the data $Dst \leq -50$ nT and the model *Dst* was not ≤ -50 nT. The type II error or "false positive" means the data was not $Dst \leq -50$ nT and the model *Dst* was ≤ -50 nT. The statistical *Dst* decisions are evaluated from Table 2 and for the rectified or Siscoe input there are 4/15 (73.3%) correct, 11/15 (26.7%) false negatives, and 0/15 (0%) false positives. For the Newell input there are 8/15 (53.3%)correct, 7/15 (46.7%) false negatives, and 0/15 (0%) false positives.

[21] WINDMI model results can be compared with a simple persistence model in which the prediction is the *AL* or *Dst* value from the previous hour. The persistence *Dst* prediction performs very well with an average ARV = 0.06 ± 0.04 and COR = 0.94 ± 0.03. These results are consistent with the *Dst* measuring the time integrated strength of the large-scale ring current which is not strongly influenced by chaotic magnetosphere processes. The *AL* persistence prediction does not perform as well as the WINDMI model with an average ARV = 0.52 ± 0.27 and COR = 0.43 ± 0.16. The *AL* index measures the smaller-scale electrojet currents which are dependent on magnetosphere turbulence and the solar wind-magnetosphere dynamic interaction and therefore the *AL* is better characterized by the WINDMI model.

4. Real-Time WINDMI Results: The 14–18 December 2006 Event

[22] ACE solar wind data for the largest event, 14–18 December 2006, is shown in Figure 1. A halo CME occurs at 0254 UT on 13 December with a projected speed of 1774 km/s and is accompanied by an X3.4 flare [*McKenna-Lawlor et al.*, 2008; *Liu et al.*, 2008]. The rectified, Siscoe, and Newell input driving voltages for this period are shown in Figure 2 and the Real-time WINDMI results, *AL*, *Dst*, and *SYM-H*, data are shown in Figure 3. There is a shock at 1352 UT on 14 December in the ACE number density and velocity data with a speed of 1030 km/s [*Liu et al.*, 2008]. Sudden storm commencement occurs at 1414

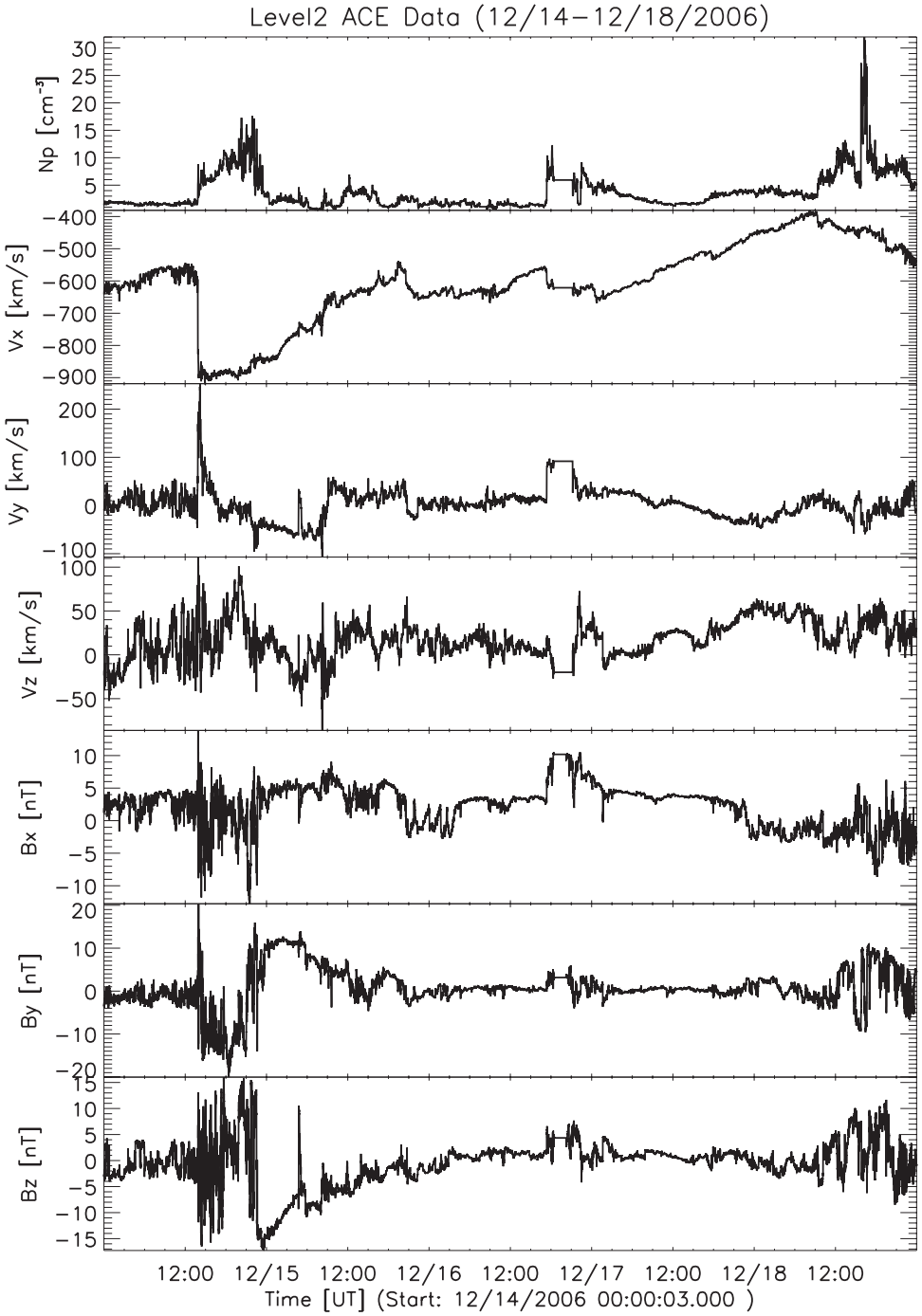

Figure 1. ACE solar wind number density, velocity, and interplanetary magnetic field data for 14−18 December 2006 in GSM coordinates show a shock at 1352 UT on 14 December with a speed of 1030 km/s.

UT on 14 December and the *Dst* reached −146 nT at 0730 UT (the midpoint of the hourly *Dst* interval) on 15 December. In recent years a new index, *SYM-H*, representing ring current development with a 1 min temporal resolution, has become available [*Iyemori*, 1990] and can be used as a higher-resolution version of *Dst* [*Wanliss and Showalter*, 2006]. On 15 December, minimum *SYM-H* reached −211 nT at 0056 UT and hourly-averaged *SYM-H* −191 nT at 0030 UT. The minimum Δ H values at the Earth due to the ring current in WINDMI are −180/−193/−228 nT for

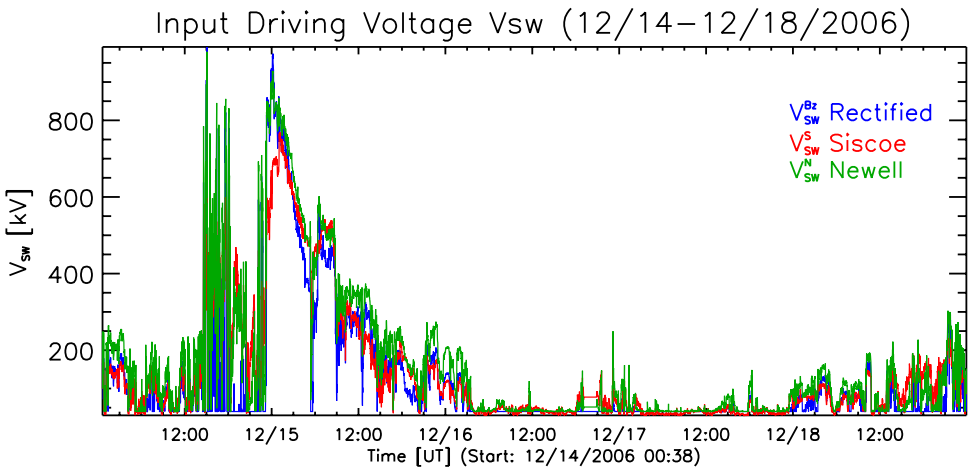

Figure 2. Rectified V_{sw}^{Bs} (blue), Siscoe V_{sw}^{S} (red), and Newell V_{sw}^{N} (green) input solar wind driving voltages for 14−18 December 2006.

the rectified/Siscoe/Newell driver voltages at 0914/0926/0924 UT, respectively, on 15 December. These values are very close to the observed minimum *SYM-H* but are significantly lower than the observed minimum *Dst*. In addition, the minima in *Dst* and *SYM-H* occurred 1.75−2 and 8.5 h earlier, respectively, than the WINDMI minimum *Dst* prediction. As a result, the ring current was well into its recovery phase by the time WINDMI predicted peak ring current energy content. The observed earlier recovery of the *SYM-H* and *Dst* compared to WINDMI is most likely due to a drop in the nightside plasma sheet density (ring current source population)

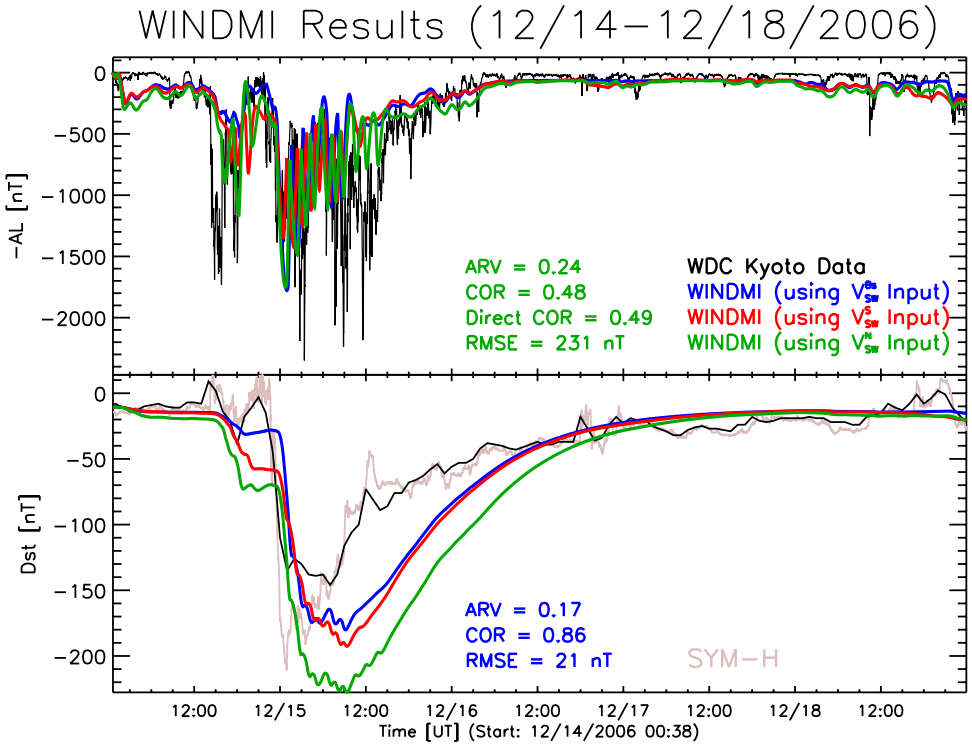

Figure 3. Real-time WINDMI *AL* and *Dst* results for 14−18 December 2006. Model results using as input the rectified voltage V_{sw}^{Bs} are shown in blue, the Siscoe voltage V_{sw}^{S} is shown in red, and the Newell voltage V_{sw}^{N} is shown in green. WDC, Kyoto, provisional *AL* and *Dst* data is shown in black and the *SYM-H* data is shown in gray.

observed by the LANL geosynchronous satellites [data from CDAWeb, courtesy of LANL]. Decreases in plasma sheet density on the nightside are known to be a contributing factor at times in the ring current decay [*Kozyra et al.*, 1998; *Liemohn et al.*, 2001; *Jordanova et al.*, 2003]; but these variations are not represented in WINDMI.

[23] The *AL* index shows much activity with large negative spikes of −1690, −1732, and −1555 nT on 14 December at 1451, 1549, and 1802 UT, and larger negative spikes of −2191, −2349, −2237, and −2183 nT on 15 December at 0246, 0324, 0852, and 1135 UT. WINDMI missed the *AL* spike at 1451 UT on 14 December associated with shock arrival. It predicted the timing and magnitude of next two *AL* spikes quite well. But then underpredicted the magnitude of the larger *AL* spikes on 15 December. This is particularly interesting because the *AL* spikes at 0324 and 0852 UT on 15 December both preceded large drops in nightside plasma sheet density that contributed to intervals of rapid ring current recovery not reproduced in WINDMI. A more detailed analysis of the reasons for discrepancies between WINDMI predictions and observations is being undertaken as a follow on to the results reported here.

5. Discussion and Conclusions

[24] For the time period between February 2006 and September 2008, 22 storm and/or substorm events are studied on the basis of forecasts with the Real-Time WINDMI model. The model has been working reliably for 2 years with an email alert system set to a threshold of −50 and −400 nT for the predicted *Dst* and *AL*, respectively.

[25] The performance of the model is evaluated for 22 events (see Table 2) with the Average Relative Variance (ARV), correlation coefficient (COR), and Root Mean Squared Error (RMSE) by comparing model results to *AL* and *Dst* data from WDC, Kyoto. The Newell input function yielded the best model *AL* predictions by all three measures (mean ARV, COR, and RMSE), followed by the rectified, then Siscoe input functions. Model *AL* predictions correlate at least one standard deviation better with the data than a direct correlation between the input coupling functions and the *AL* index.

[26] The rectified input has the best mean *Dst* ARV by a percent difference of 13% and 37% from the mean *Dst* ARV of the Siscoe and Newell inputs, respectively. The mean *Dst* COR and RMSE measures do not readily distinguish between the three input coupling functions. The solar wind input driver which produces the best *Dst* and *AL* WINDMI model predictions are different for each index. This suggests that different solar wind-magnetosphere coupling physics may be responsible for producing the electrojet and ring current.

[27] *Spencer et al.* [2009] show that the Newell input function yields slightly better *Dst* results and the rectified input slightly better *AL* results when used with an optimized parameter set. However, their study was for large geomagnetic activity of long duration (15–24 April 2002) for which the input coupling functions were evaluated after WINDMI model parameter optimization on a large previous event (3–7 October 2000).

[28] This study can be extended to evaluate the performance of the model using other input driving voltages and for optimized WINDMI parameters. The database of Real-Time WINDMI *Dst* predictions can also be compared with other ring current models which contain different loss and energization processes.

[29] Some model enhancements in development include adding more physics to the calculation of the *Dst* due to tail current increases, and *Dst* sudden commencement features which are being modeled by computing compression of the dayside magnetopause. The model is also in the process of being extended to include the dayside magnetosphere current systems which would provide a model AU prediction.

Appendix A: Measures of Performance

[30] For a time series $i = 1, 2, \ldots N$ of predicted model values x_i and observed data values y_i, three measures of the agreement between the model and the data are used.

[31] The average relative variance (ARV) is the primary measure used and is given by

$$ARV = \frac{\Sigma_i (x_i - y_i)^2}{\Sigma_i (\overline{y} - y_i)^2}. \quad \text{(A1)}$$

The ARV approaches zero when the model output and data converge to each other. When the ARV is equal to one then the model is only as good as the average of the data. The prediction efficiency (PE) is given by $PE = 1 - ARV$.

[32] The correlation coefficient (COR) is given by

$$COR = \frac{\Sigma_i (x_i - \overline{x})(y_i - \overline{y})}{\sigma_x \sigma_y} \quad \text{(A2)}$$

and is a measure of how well correlated the model is to the data with $COR = 0$ meaning they are uncorrelated, $COR > 0$ for a positive correlation, and $COR < 0$ for a negative correlation. The root mean squared error (RMSE) quantifies the amount by which the model differs from the data and is given by

$$RMSE = \sqrt{\Sigma_i (x_i - y_i)^2 / N}. \quad \text{(A3)}$$

The RMSE has the units of the data (nT) and thus is useful for inferring the range of uncertainty in the predicted signal. Small RMSE values are indications of model results in good agreement with data.

[33] **Acknowledgments.** This work was partially supported by NSF grants ATM-0638480, ATM-0720201, ATM-0402163, and NASA grants NNG05GJ89G, NNG05GM48G, NNX08AV83G, and NNX08AQ15G. The solar wind plasma

and magnetic field data were obtained from NOAA's ACE RTSW site. The geomagnetic indices used were obtained from the World Data Center for Geomagnetism, Kyoto, Japan. MPA density data was obtained from CDAWeb (http://cdaweb.gsfc.nasa.gov), courtesy of LANL, and we thank Michelle Thomsen for helpful comments. The SOHO LASCO CME catalog is generated and maintained at the CDAW Data Center by NASA and The Catholic University of America in cooperation with the Naval Research Laboratory. SOHO is a project of international cooperation between ESA and NASA. Sudden storm commencement data were obtained from NOAA NGDC (http://www.ngdc.noaa.gov/stp/SOLAR/ftpSSC.html).

References

Bargatze, L. F., D. N. Baker, R. L. McPherron, and J. E. W. Hones (1985), Magnetospheric impulse response for many levels of geomagnetic activity, *J. Geophys. Res.*, *90*(A7), 6387–6394.

Bargatze, L. F., R. L. McPherron, J. Minamora, and D. Weimer (2005), A new interpretation of Weimer et al.'s solar wind propagation delay technique, *J. Geophys. Res.*, *110*, A07105, doi:10.1029/2004JA010902.

Burton, R. K., R. L. McPherron, and C. T. Russell (1975), An empirical relationship between interplanetary conditions and *Dst*, *J. Geophys. Res.*, *80*, 4204–4214.

Dessler, A., and E. N. Parker (1959), Hydromagnetic theory of geomagnetic storms, *J. Geophys. Res.*, *64*, 2239–2259.

Horton, W., and I. Doxas (1996), A low-dimensional energy-conserving state space model for substorm dynamics, *J. Geophys. Res.*, *101*(A12), 27,223–27,237.

Horton, W., and I. Doxas (1998), A low-dimensional dynamical model for the solar wind driven geotail-ionosphere system, *J. Geophys. Res.*, *103*(A3), 4561–4572.

Iyemori, T. (1990), Storm-time magnetospheric currents inferred from mid-latitude geomagnetic field variations, *J. Geomagn. Geoelectr.*, *42*, 1249–1265.

Jordanova, V. K., L. M. Kistler, M. F. Thomsen, and C. G. Mouikis (2003), Effects of plasma sheet variability on the fast initial ring current decay, *Geophys. Res. Lett.*, *30*(6), 1311, doi:10.1029/2002GL016576.

Klimas, A., D. Baker, D. Roberts, D. Fairfield, and J. Buchner (1992), A nonlinear dynamical analogue model of geomagnetic activity, *J. Geophys. Res.*, *97*(A8), 12,253–12,266.

Klimas, A. J., D. N. Baker, D. Vassiliadis, and D. A. Roberts (1994), Substorm recurrence during steady and variable solar wind driving: Evidence for a normal mode in the unloading dynamics of the magnetosphere, *J. Geophys. Res.*, *99*, 14,855–14,862, doi:10.1029/94JA01240.

Klimas, A. J., D. Vassiliadis, and D. N. Baker (1998), *Dst* index prediction using data-derived analogues of the magnetospheric dynamics, *J. Geophys. Res.*, *103*, 20,435–20,448, doi:10.1029/98JA01559.

Kozyra, J. U., V. K. Jordanova, J. E. Borovsky, M. F. Thomsen, D. J. Knipp, D. S. Evans, D. J. McComas, and T. E. Cayton (1998), Effects of a high-density plasma sheet on ring current development during the November 2–6, 1993, magnetic storm, *J. Geophys. Res.*, *103*, 26,285–26,306, doi:10.1029/98JA01964.

Li, X., K. S. Oh, and M. Temerin (2007), Prediction of the *AL* index using solar wind parameters, *J. Geophys. Res.*, *112*, A06224, doi:10.1029/2006JA011918.

Liemohn, M. W., J. U. Kozyra, M. F. Thomsen, J. L. Roeder, G. Lu, J. E. Borovsky, and T. E. Cayton (2001), Dominant role of the asymmetric ring current in producing the stormtime *Dst**, *J. Geophys. Res.*, *106*, 10,883–10,904, doi:10.1029/2000JA000326.

Liu, Y., et al. (2008), A comprehensive view of the 2006 December 13 CME: From the Sun to interplanetary space, *Astrophys. J.*, *689*, 563–571.

McKenna-Lawlor, S. M. P., et al. (2008), Predicting interplanetary shock arrivals at Earth, Mars, and Venus: A real-time modeling experiment following the solar flares of 5–14 December 2006, *J. Geophys. Res.*, *113*, A06101, doi:10.1029/2007JA012577.

Newell, P. T., T. Sotirelis, K. Liou, and F. J. Rich (2007), A nearly universal solar wind-magnetosphere coupling function inferred from 10 magnetospheric state variables, *J. Geophys. Res.*, *112*, A01206, doi:10.1029/2006JA012015.

Newell, P. T., T. Sotirelis, K. Liou, and F. J. Rich (2008), Pairs of solar wind-magnetosphere coupling functions: Combining a merging term with a viscous term works best, *J. Geophys. Res.*, *113*, A04218, doi:10.1029/2007JA012825.

Ober, D. M., N. C. Maynard, and W. J. Burke (2003), Testing the Hill model of transpolar potential saturation, *J. Geophys. Res.*, *108*(A12), 1467, doi:10.1029/2003JA010154.

O'Brien, T. P., and R. L. McPherron (2000), An empirical phase space analysis of ring current dynamics: Solar wind control of injection and decay, *J. Geophys. Res.*, *105*, 7707–7720, doi:10.1029/1998JA000437.

Reiff, P. H., and J. G. Luhmann (1986), Solar wind control of the polar-cap voltage, in *Solar Wind-Magnetosphere Coupling*, edited by Y. Kamide and J. A. Slavin, pp. 453–476, Terra Sci, Tokyo.

Rostoker, G. (1972), Geomagnetic indices, *Rev. Geophys. Space Phys.*, *10*, 935–950.

Shue, J.-H., J. K. Chao, H. C. Fu, C. T. Russell, P. Song, K. K. Khurana, and H. J. Singer (1997), A new functional form to study the solar wind control of the magnetopause size and shape, *J. Geophys. Res.*, *102*, 9497–9512, doi:10.1029/97JA00196.

Siscoe, G. L., N. U. Crooker, and K. D. Siebert (2002a), Transpolar potential saturation: Roles of region-1 current system and solar wind ram pressure, *J. Geophys. Res.*, *107*(A10), 1321, doi:10.1029/2001JA009176.

Siscoe, G. L., G. M. Erickson, B. U. O. Sonnerup, N. C. Maynard, J. A. Schoendorf, K. D. Siebert, D. R. Weimer, W. W. White, and G. R. Wilson (2002b), Hill model of transpolar potential saturation: Comparisons with MHD simulations, *J. Geophys. Res.*, *107*(A6), 1075, doi:10.1029/2001JA000109.

Spencer, E., W. Horton, M. L. Mays, I. Doxas, and J. Kozyra (2007), Analysis of the 3–7 October 2000 and 15–24 April 2002 geomagnetic storms with an optimized nonlinear dynamical model, *J. Geophys. Res.*, *112*, A04S90, doi:10.1029/2006JA012019.

Spencer, E., A. Rao, W. Horton, and M. L. Mays (2009), Evaluation of solar wind-magnetosphere coupling function during geomagnetic storms with the WINDMI model, *J. Geophys. Res.*, *114*, A02206, doi:10.1029/2008JA013530.

Stone, E. C., A. M. Frandsen, R. A. Mewaldt, E. R. Christian, D. Margolies, J. F. Ormes, and F. Snow (1998), The Advanced Composition Explorer, *Space Sci. Rev.*, *86*, 1–22.

Sugiura, M. (1964), Hourly values of equatorial *Dst* for the IGY, *Ann. Int. Geophys. Year*, *35*(9), 945–948.

Temerin, M., and X. Li (2002), A new model for the prediction of *Dst* on the basis of the solar wind, *J. Geophys. Res.*, *107*(A12), 1472, doi:10.1029/2001JA007532.

Temerin, M., and X. Li (2006), *Dst* model for 1995–2002, *J. Geophys. Res.*, *111*, A04221, doi:10.1029/2005JA011257.

Wanliss, J. A., and K. M. Showalter (2006), High-resolution global storm index: *Dst* versus *SYM-H*, *J. Geophys. Res.*, *111*, A02202, doi:10.1029/2005JA011034.

Weimer, D., D. Ober, N. Maynard, M. Collier, D. McComas, N. Ness, C. Smith, and J. Watermann (2003), Predicting interplanetary magnetic field (IMF) propagation delay times using the minimum variance technique, *J. Geophys. Res.*, *108*(A1), 1026, doi:10.1029/2002JA009405.

W. Horton and M. L. Mays, Institute for Fusion Studies, University of Texas at Austin, 1 University Station, C1500, Austin, TX 78712-0262, USA. (lmays@physics.utexas.edu)

J. Kozyra, Department of Atmospheric, Oceanic, and Space Sciences, University of Michigan, 2455 Hayward Street, Ann Arbor, MI 48109-2143, USA.

E. Spencer, Center for Space Engineering, Utah State University, 4170 Old Main Hill, EL 214, Logan, UT 84322-4170, USA.